Applied Catalysis B: Environmental 218 (2017) 480–487

Contents lists available at ScienceDirect

Applied Catalysis B: Environmental

journal homepage: www.elsevier.com/locate/apcatb

Visible light photocatalysis over solid acid: Enhanced by gold plasmonic effect

Feng Lin[a,b], Bin Shao[a], Zhen Li[c], Junying Zhang[a], Huan Wang[a], Shaohua Zhang[a], Masatake Haruta[a,d,**], Jiahui Huang[a,*]

[a] Gold Catalysis Research Center, State Key Laboratory of Catalysis, Dalian Institute of Chemical Physics, Chinese Academy of Sciences, 457 Zhongshan Road, Dalian 116023, China
[b] Key Laboratory of New Energy and Rare Earth Resource Utilization, State Ethnic Affairs Commission, School of Physics and Materials Engineering, Dalian Minzu University, Dalian 116600, China
[c] Dalian National Laboratory for Clean Energy, Dalian Institute of Chemical Physics, Chinese Academy of Sciences, 457 Zhongshan Road, Dalian 116023, China
[d] Research Center for Gold Chemistry, Department of Applied Chemistry, Graduate School of Urban Environmental Sciences, Tokyo Metropolitan University, 1-1 Minami-Osawa, Hachioji, Tokyo 192-0397, Japan

ARTICLE INFO

Article history:
Received 5 April 2017
Received in revised form 23 June 2017
Accepted 25 June 2017
Available online 27 June 2017

Keywords:
Au SPR
SO_4^{2-}–TiO_2
Surface acidity
Pollutant
Photocatalytic oxidation

ABSTRACT

Solar driven catalysis by semiconductors is considered as a promising route to mitigate environmental problems caused by the combustion of fossil fuels and water pollution. Surface plasmon resonance (SPR) has offered a new opportunity to overcome the limited efficiency of photocatalysts. Herein we report that the SPR-mediated visible-light-responsive photocatalyst, 0.5 wt.% Au/SO_4^{2-}–TiO_2, can achieve over 99% conversion of pollutants (thiophene, thiol, rhodamine B, and phenol) during photocatalytic oxidation with oxygen or air as oxidant under visible light irradiation. The considerable enhancement of photocatalytic activity can be attributed to the synergistic effect of Au SPR and Lewis acidic SO_4^{2-}–TiO_2 which are beneficial for the efficient separation and transfer of the photo-generated electrons and holes. Such a strategy would be important to the design and preparation of highly photocatalytic active semiconductor catalysts.

1. Introduction

Solar driven catalysis on semiconductors is widely considered as a promising route to mitigate environmental problems caused by the combustion of fossil fuels and water pollution [1,2]. SO_x produced from the automobile exhaust gas *via* the burning of sulfur-containing components present in fuels results in serious air pollution. Thiophene and thiol are the typical representatives among the sulfur-containing components. Thiophene with the aromaticity and the low electron density on sulfur atom is the most difficult to oxidize with conventional oxidative desulfurization processes [3]. Several effective photocatalysts are reported for the photocatalytic desulfurization [4–7]. Besides, polluted wastewater from industry is a globally environmental problem. The mitigation of azo dyes rhodamine B (RhB) and toxic chemicals (*e.g.* phenol) induced by the industry is necessary for the environmental pollution control. Consequently, several materials that enable the cleanup of polluted water *via* a far less aggressive approach are developed [8,9].

Titania-based catalyst as one of the most photoactive semiconductor catalysts has been extensively investigated. TiO_2 exhibits high activity and stability, and has proven to be an excellent photocatalyst material under UV light exposure [10,11]. The photocatalytic activity of TiO_2 varies significantly with its phase structure, crystallinity and particle size [12–14]. Various methods have been employed to control the crystal phases of TiO_2 [15–19]. Li et al. [20] investigated the photocatalytic reforming of methanol on Pt/TiO_2–SO_4^{2-} as a model reaction of biomass reforming. TiO_2–SO_4^{2-} with a tunable surface phase was prepared by

* Corresponding author at: Gold Catalysis Research Center, State Key Laboratory of Catalysis, Dalian Institute of Chemical Physics, Chinese Academy of Sciences, 457 Zhongshan Road, Dalian 116023, China.
** Corresponding author at: Gold Catalysis Research Center, State Key Laboratory of Catalysis, Dalian Institute of Chemical Physics, Chinese Academy of Sciences, 457 Zhongshan Road, Dalian 116023, China. Research Center for Gold Chemistry, Department of Applied Chemistry, Graduate School of Urban Environmental Sciences, Tokyo Metropolitan University, 1-1 Minami-Osawa, Hachioji, Tokyo 192-0397, Japan.
E-mail addresses: haruta-masatake@center.tmu.ac.jp (M. Haruta), jiahuihuang@dicp.ac.cn (J. Huang).

http://dx.doi.org/10.1016/j.apcatb.2017.06.076
0926-3373/

calcining commercially available TiO_2 with deposited sodium sulfate Na_2SO_4 as a modifier. Colon et al. [21] used a sol-gel method to synthesize the sulfated TiO_2. They found that SO_4^2 could maintain the anatase phase of TiO_2. However, the sulfated TiO_2 was mainly used in the photocatalytic esterification reaction and oxidation of alcohols/pollutants [22–24].

On the other hand, it was reported that the deposition of noble metal such as Pt, Ag, and RuO_2 as cocatalysts on TiO_2 [25,26] greatly improved the activity of the photocatalysts [27,28]. Very recently, we found that photocatalyst RuO_2/SO_4^{2-}–TiO_2 could display the excellent photocatalytic activity in thiophene oxidation [29,30]. The synergistic effect of RuO_2 as an oxidation cocatalyst and Lewis acidic SO_4^{2-}–TiO_2 which capture superoxide species/activate thiophene molecules is beneficial for the efficient photocatalytic oxidation of thiophene. The co-existing oxidation cocatalyst and lewis acid site offer a more promising approach for the photocatalytic oxidation of pollutants. The recent development of surface plasmon resonance (SPR) has offered a new opportunity to overcome the limited efficiency of photocatalysts. SPR improves the solar-energy-conversion efficiency by (i) expanding light absorption to longer wavelengths, (ii) increasing light scattering, and (iii) exciting electron–hole pairs in the semiconductor by transferring the plasmonic energy from the metal to the semiconductor [31,32]. The deposition of plasmonic metal nanoparticles (NPs) on semiconductors can enhance photocatalytic activity toward water splitting and organic compound degradation [33–41].

In process (iii), the concentrated energy contained in localized plasmonic oscillations is transferred to the semiconductor, inducing charge separation in the semiconductor. So far, the SPR-induced charge separation mechanism remains unclear. It is reported as the direct electron transfer (DET), SPR-mediated local electromagnetic field (LEMF) and resonant energy transfer (RET) process. DET depends on the alignment of the band levels of the semiconductor and Fermi level of the plasmonic metal. DET occurs after the excitation and subsequent decoherence of the SPR, which leaves a population of hot electrons that are able to transfer to the semiconductor. LEMF and RET process lead to the charge separation and create carriers in the semiconductor which is in favor of high photocatalytic activity [31,32].

Herein we report the photocatalytic oxidation of thiol, thiophene, RhB, and phenol by a SPR-mediated visible-light responsive photocatalyst Au/SO_4^{2-}–TiO_2 (Au/ST). An extraordinary photocatalytic activity (over 99% conversions of pollutants) can be achieved under visible light irradiation ($\lambda \geq 420$ nm). We find the synergistic effect of Au SPR and Lewis acidic SO_4^{2-}–TiO_2 is beneficial for the highly efficient photocatalytic oxidation of pollutants.

2. Experimental

2.1. Catalyst preparation

All chemicals used in these experiments were of analytical reagent grade. The solid acid SO_4^{2-}–TiO_2 catalysts were prepared by incipient wetness method [7]. TiO_2 (Degussa P25) was submerged in a nM H_2SO_4 solution (n = 0.5, 1–3). The mixture was heated at 50 °C to evaporate water and then calcined at 450 °C for 3 h to obtain the solid acid SO_4^{2-}/TiO_2. Solid-acid SO_4^{2-}–TiO_2 catalysts were denoted as n ST (n = 0.5, 1–3 M H_2SO_4, ST = SO_4^{2-}–TiO_2).

The deposition of Au NPs on solid acid ST was prepared as follows. A certain amount of polyvinyl alcohol (PVA) aqueous solution was added to an aqueous solution of $HAuCl_4$ under vigorous stirring. Then an excessive $NaBH_4$ was rapidly added ($NaBH_4$/Au (mol/mol) = 5), resulting in the chemical reduction of Au^{3+} cations. The color of the solution immediately changed from light yellow to dark red, indicating the formation of Au sol. After stirring for 1 h, the required amount of the solid acid ST was added to Au sol in order to obtain an i wt.% Au loaded ST catalyst (i = 0.1, 0.5, 1.0, 2.0). The pH value of solution was 1–2 after the addition of solid acid ST. After the vigorous stirring for 2 h, the catalyst was filtrated, washed thoroughly with distilled water and dried at 80 °C under vacuum for 24 h. The as prepared i wt.% Au/SO_4^{2-}–TiO_2 was denoted as i Au/ST. In some cases, i Au/ST was further calcined at 300 °C in air to remove PVA.

2.2. Catalyst characterization

The prepared samples were characterized by X-ray powder diffraction (XRD) on a Rigaku D/Max-2500/PC powder diffractometer. Each sample was scanned using Cu-K_α radiation with an operating voltage of 40 kV and an operating current of 200 mA. The scan rate of 5° min^{-1} was applied to record the patterns in the range of 10–80° at a step of 0.02°. UV–vis diffuse reflectance spectra (UV–vis DRS) were recorded on a UV–vis spectrophotometer (PerkinElmer Lambda 750) equipped with an integrating sphere. Transmission Electron Microscopy (TEM) was used to examine the size of Au NPs. The TEM images were obtained on a Quanta 200F microscope (FEI Company) with the accelerating voltage of 0.5–30 kV and a Tecnai G2 Spirit microscopy (FEI Company) with the accelerating voltage of 120 kV. A FEI Tecnai G2 F20 transmission electron microscope (TEM) equipped with a high-angle annular dark field scanning TEM (HAADF-STEM) detector operated at 200 kV was utilized to observe Au NPs. Inductively coupled plasma optical emission spectrometry (ICP-OES) was carried out on a 7300 DV (Perkin Elmer) ICP OES spectrophotometer. X-ray photoelectron spectroscopy (XPS) was acquired on Thermo ESCALAB 250Xi with an Al Ka X-ray ($h\nu$ = 1486.6 eV).

Mott-Schottky (MS) analysis was carried out at a DC potential range 0–1 V *vs.* RHE with an AC potential frequency of 1 kHz under dark condition. The fabricated electrode, a platinum electrode, and saturated calomel electrode (RHE) were used as working, counter and reference electrodes, respectively. If there is no special mention, 0.5 M Na_2SO_4 aqueous solution (pH 6.8) was used as an electrolyte after saturation with Ar gas for 30 min.

The nitrogen adsorption-desorption isotherms were obtained at −196 °C with a micromeritics ASAP 2020 apparatus. Prior to the measurement the samples were outgassed at 250 °C for 6 h. Specific surface area determination was based on BET formalism. The mesopore size distributions were calculated from the desorption branch.

ESR signals of radicals trapped by DMPO were recorded at ambient temperature on a Brucker ESR A200 spectrometer. After bubbling O_2 for 10 min, the samples were introduced into the homemade quartz cup inside the microwave cavity and illuminated with a 300 W Xe lamp (CERAMAX LX-300). The settings for the ESR spectrometer were as follows: center field, 3486.7 G; sweep width, 100 G; microwave frequency, 9.8 GHz; modulation frequency, 200 kHz; power, 10.0 mW. Magnetic parameters of the radicals detected were obtained from direct measurements of magnetic field and microwave frequency.

2.3. Photocatalytic reaction

The photocatalytic reactions of thiophene and thiol were carried out in a Pyrex reaction cell with O_2 or air bubbling at a constant flow rate. Photocatalyst (1 g L^{-1}) was dispersed in an acetonitrile solution containing given amounts of thiophene ($[\text{sulfur content}]_{initial}$ = 600 ppm). The suspension was irradiated by a 300 W Xe lamp (CERAMAX LX-300), which is equipped with an optical filter ($\lambda \geq 420$ nm) to cut off the light in the ultraviolet region. The temperature of the reaction solution was maintained at 10 ± 2 °C

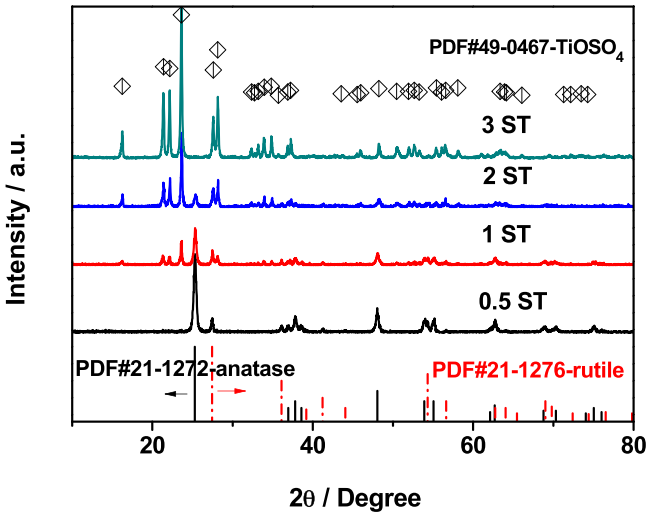

Fig. 1. The XRD patterns of ST supports, the standard card of anatase (No. 21-1272), rutile (No. 21-1276) and $TiOSO_4$ (No. 49-0467).

Table 1
Textural properties of TiO_2 and n ST supports determined by N_2 physisorption.

	TiO_2 (P25)	0.5 ST	1 ST	2 ST	3 ST
BET surface area/$m^2\,g^{-1}$	47.0	36.0	1.8	3.0	4.4
Pore volume/$cm^3\,g^{-1}$	0.148	0.269	0.001	0.018	0.035
Pore diameter/nm	12.6	30.4	24.3	24.3	32.1

by a flow of cooling water. The products were analyzed by GC-FPD (Agilent 7890, pona column).

The photocatalytic degradation reactions of dye rhodamine B (RhB) and phenol were carried out in a Pyrex reaction cell. Photocatalyst ($1\,g\,L^{-1}$) was dispersed in an aqueous solution containing given amounts of the pollutants ($C_0 = 5$ ppm). The temperature of the reaction solution was maintained at $10 \pm 2\,^{\circ}C$ by a flow of cooling water. The concentration of RhB and phenol was monitored by colorimetry with a JASCO V-550 UV–vis spectrometer. The λ_{max} for RB and phenol are 553 and 270 nm, respectively. Calibration based on the Beer-Lambert law was used to quantify the dye concentration.

3. Results and discussion

3.1. Characterization of photocatalysts

Fig. 1 shows the XRD patterns of n ST supports and standard cards of anatase, rutile and titanyl sulfate ($TiOSO_4$). For 0.5 ST, the diffraction peaks are assigned to anatase and rutile, and the typical phase structure of TiO_2 (P25) is well preserved. As the acid concentration in the preparation of ST samples increases, the diffraction peaks attributed to $TiOSO_4$ appear and their intensity become stronger and stronger. The $TiOSO_4$ phase becomes the main phase structure in 2 ST and 3 ST. For 3 ST, the diffraction peaks assigned to anatase and rutile nearly disappear. Clearly, the TiO_2 phase structure can be tuned by the sulfation process and the $TiOSO_4$ phase will be the main phase structure in ST samples.

As shown in Table 1, n ST supports show relatively low BET surface area ($1.8–36.0\,m^2\,g^{-1}$) and pore volumes ($0.001–0.269\,cm^3\,g^{-1}$) compared with P25. As the surface acidity increases, the surface area and pore volume of n ST decrease rapidly and reach a minimum of $1.8\,m^2\,g^{-1}$ and $0.001\,cm^3\,g^{-1}$ for 1 ST, and then increase slowly for 2 ST and 3 ST. On the other hand, the pore diameter of catalysts increases obviously after the sulfation (24.3–32.1 nm). In our previous work [7], the photocatalytic oxidation investigation of thiophene showed that 1 ST and 2 ST were the most effective photocatalysts. FT-IR spectroscopy of pyridine adsorption indicated that the surface acidity property of photocatalysts is critical issue for photocatalytic activity of thiophene oxidation. Compared with 1 ST, 2 ST has the higher surface area and bigger pore volume (Table 1). Considering that the high surface area and big pore volume are beneficial to enhance the absorption of reaction molecules and then the catalytic activity, herein 2 ST is chosen to support Au NPs for catalytic investigation.

Fig. 2 shows the TEM images, HAADF-STEM images and Au particle size distributions of Au-sol, Au/2 ST, Au/2 ST after the photocatalytic oxidation reaction and Au/2 ST after the calcination. Fig. 2a and b shows that the Au-sol is relative homogenous, which display a narrow size distribution with a mean size of 2.9 nm (Fig. 2c). After loaded on 2 ST, Au NPs are highly dispersed on the surface of 2 ST (Fig. 2d and e). The mean size of Au NPs and the typical size of 2 ST are estimated to be 5.1 nm (Fig. 2f) and 20–25 nm, respectively. After the further photocatalytic reaction, the mean size of Au NPs is slightly grown to 7.0 nm, and a broader size distribution is also observed (Fig. 2g–i). After calcination at 300 °C in air, some Au NPs are kept stable, but the others aggregate to form 10–15 nm Au NPs, finally giving a mean size of 10.7 nm (Fig. 2–l). X-ray photoelectron spectroscopy (XPS) of fresh Au/2 ST catalyst displays typical peaks of Au 4f and Ti^{4+} 2p, respectively (Fig. S1a, b). The results indicate that Au species exist as metallic state in the surface of ST catalyst, and Ti species are mainly as +4 chemical valence state.

Fig. 3a shows the UV–vis diffuse reflectance spectra of 2 ST and Au/2 ST with different Au loadings. 2 ST shows a strong absorption in the ultraviolet light region until about 400 nm, almost the same as TiO_2. So 2 ST is a UV-light-responsive material. Interestingly, when the Au NPs are loaded on 2 ST, there is a little red shift of the absorption edges, and the new absorption bands centered at 550 nm could be observed on the absorption curves. The absorption spectra are expanded to visible light region and even to the infrared light region near 700 nm. Such strong absorption throughout the visible to near-infrared light range is caused by the Au SPR effect. This process concentrates the incident photon energy in plasmon oscillations. Then the concentrated energy contained in localized plasmonic oscillations will be transferred to the semiconductor 2 ST, inducing the charge separation in ST catalysts. In short, Au/2 ST can absorb the visible light and even the infrared light, and thus is expected as an effective visible-light-responsive photocatalyst ($\lambda \geq 420$ nm). The visible-photocurrent of 0.5Au/2 ST electrode indicates the importance of Au NPs for visible light absorption and charge separation during the photo-electrocatalytic process, which also reveals the function of Au NPs in photocatalytic reaction (Supporting Information, Fig. S2).

The energy band gap E_g of 0.5 Au/2 ST can be calculated from the UV–vis diffuse reflectance spectra shown in Fig. 3a using equation,

$$E_g = hc/\lambda$$

Where h is the Planck's constant, c is light velocity, and λ is the absorption edge of 0.5 Au/2 ST (ca. 404 nm). The band gap energy is calculated as 3.07 eV for 0.5 Au/2 ST.

To gain more insight into the principle of this Au SPR catalyst, we investigated the electrochemical behavior to determine the potential of conduction band of 0.5 Au/2 ST. Fig. 3b displays the Mott-Schottky (MS) plot for 0.5 Au/2 ST photoelectrode. The positive slops of MS curve as well as anodic photocurrent during PEC measurements suggest n-type semiconductivity. The flat band potential is then determined by extrapolating the linear region of MS curve down to the potential axis, which reads to be 0.03 V. Accordingly, the band edge position (*i.e.* conduction band (CB) and

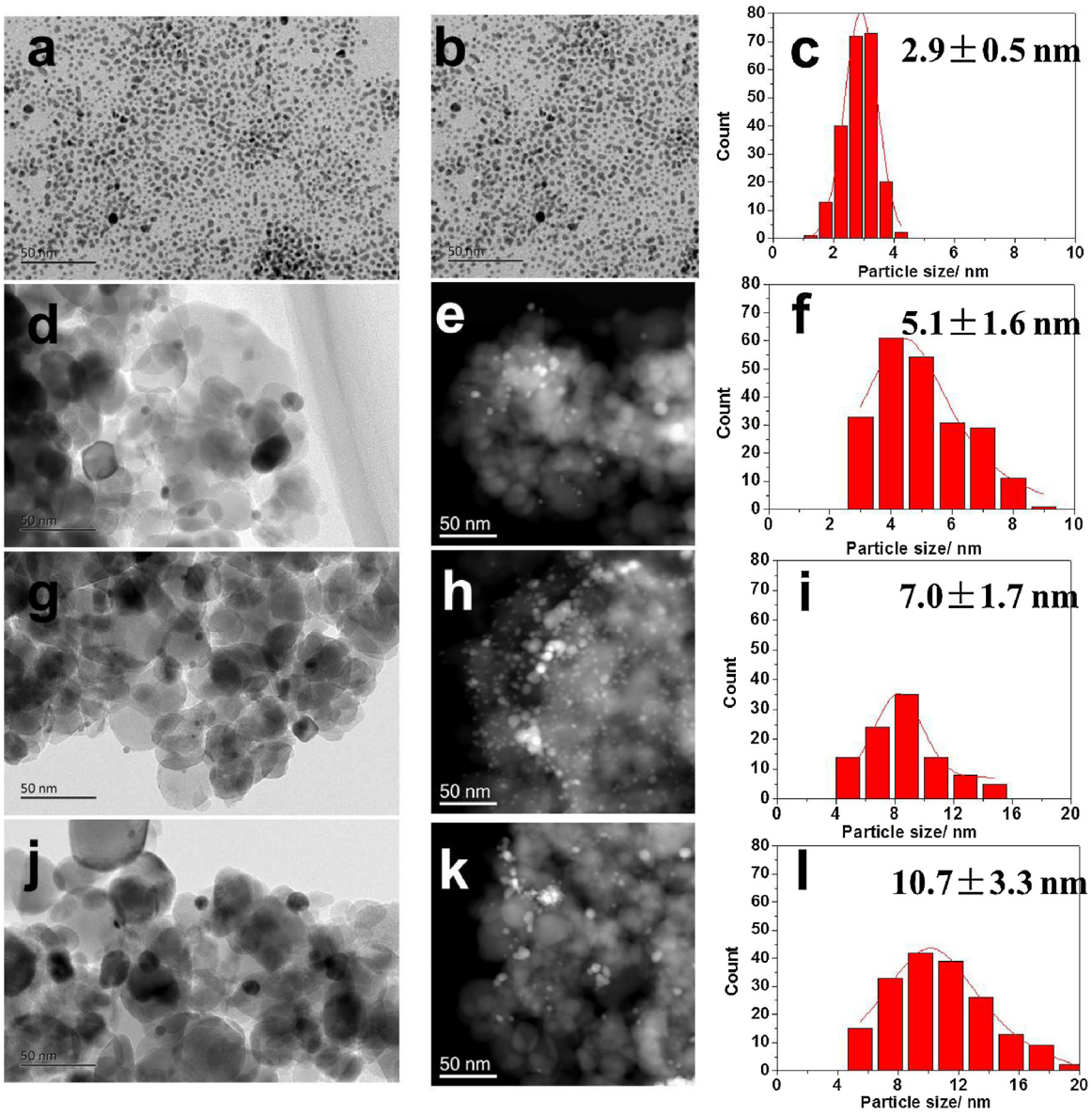

Fig. 2. TEM images, HAADF-STEM iamges and Au NPs size distributions of Au-sol (a–c), Au/2 ST (d–f), Au/2 ST after the photocatalytic reaction (g–i) and Au/2 ST after the calcinations (j–l). (Herein the nominal loadings of Au is 0.5 wt.%).

valence band (VB) edges) can be easily inferred with the aid of UV–vis spectra data. Thus the potential of conduction and valence bands of 0.5 Au/2 ST are −0.17 eV and 2.90 eV, respectively.

3.2. *Effect of Au SPR on catalytic activities of photocatalysts*

2 ST loaded with different Au loadings were synthesized in this work. ICP was used to determine the actual Au loadings. The results in Table 2 show that actual Au loadings on 2 ST are 0.11 wt.%, 0.58 wt.%, 1.18 wt.% and 2.21 wt.% for 0.1 Au/2 ST, 0.5 Au/2 ST, 1.0 Au/2 ST and 2.0 Au/2 ST, respectively, slightly higher than the nominal values. Table 2 also shows that the catalytic activities of 2 ST, fresh i Au/2 ST without calcination, 2nd cycle of i Au/2 ST without calcinations, and i Au/2 ST calcined at 300 °C in the photocatalytic oxidation of thiophene. Although 2 ST does not work in the visible light irradiation ($\lambda \geq 420$ nm), which is consistent with the light adsorption spectrum in Fig. 3, 2 ST exhibits superior photocatalytic activity for thiophene oxidation than TiO_2 (thiophene conversion, 39.2% on 2 ST *vs.* 12.3% on P25) in the irradiation by the 300 W Xe lamp (CERAMAX LX-300) without any optical filter. Compared with 2 ST, the enhancement of the photocatalytic activity of i Au/2 ST catalyst by the SPR effect of Au NPs is very appreciable. For the three sets of Au/2 ST catalysts (fresh, 2nd used and calcined) in Table 2, the highest conversion of thiophene is achieved at the Au loading of 0.5 wt.%. Lower and higher Au loading than 0.5 wt.% will cause the decrease of thiophene conversion. When the Au loading is higher than 0.5 wt.%, the amount of Au NPs may become excessive and thus cover more active sites on the surface of semiconductor ST, which may prevent the contact of reaction molecules/superoxide species with the ST surface. This may cause the decay of photocatalytic activities.

On the other hand, the photocatalytic activity of 2nd used i Au/2 ST catalysts is almost the same as that of fresh i Au/ST catalysts, but the photocatalytic activity of i Au/2 ST calcined at 300 °C is much poorer than that of fresh i Au/2 ST catalysts and 2nd used of i Au/2 ST catalysts. In particular, for 0.5 Au/ST, the conversion of thiophene can reach as high as 99.8% for the first cycle, and 100% for the second cycle, but decreases to *ca.* 95.0% after calcination. Fig. 2g and h shows that the size of Au NPs loaded on the used 0.5 Au/2 ST catalyst increases slightly from 5.1 nm to 7.0 nm compared with fresh

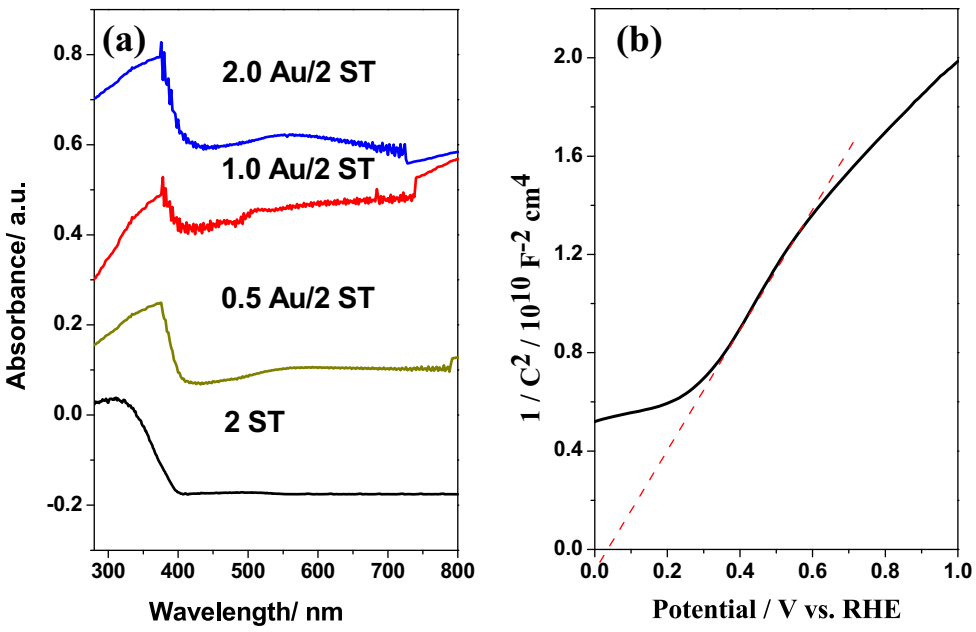

Fig. 3. (a) UV–vis diffuse reflectance spectra of 2 ST and Au/2 ST with different Au loadings, (b) MS plot of 0.5 Au/2 ST film on FTO with the AC potential frequency of 1000 Hz.

Table 2
Effect of Au loadings on catalytic activities of Au/2 ST in photocatalytic oxidation of thiophene.

Samples	Nominal Au loadings/wt.%	Actual Au loading/wt.%	Thiophene conv. in 3 h/%		
			Freshcatalyst	2nd used catalyst	Calcined catalyst
2 ST[a]	–	–	5.2	5.3	–
2 ST[b]	–	–	39.2	17.3	39.2
2 ST[c]	–	–	5.2	4.9	5.2
0.1 Au/2 ST[c]	0.1	0.11	90.0	91.0	88.0
0.5 Au/2 ST[c]	0.5	0.58	99.8	100.0	95.0
1.0 Au/2 ST[c]	1.0	1.18	93.0	90.0	86.0
2.0 Au/2 ST[c]	2.0	2.21	89.0	89.1	71.0

[a] No light irradiation.
[b] The photocatalytic reaction was irradiated by a 300W Xe lamp (CERAMAX LX-300) without any optical filter.
[c] The photocatalytic reaction was irradiated by a 300W Xe lamp (CERAMAX LX-300) equipped with an optical filter ($\lambda \geq 420$ nm) to cut off the light in the ultraviolet region.

Table 3
The catalytic stability of 0.5 Au/2 ST in photocatalytic oxidation of thiophene.

Catalyst: 0.5 Au/2 ST	Cycle test						
	Fresh	2nd used	3rd used	4th used	5th used	6th used	7th used
Thiophene conv. in 3 h/%	99.8	100.0	99.2	95.5	90.1	82.3	70.0

0.5 Au/2 ST catalyst. However, after calcination at 300 °C in air, the size of Au NPs loaded on 0.5 Au/2 ST grows significantly from 5.1 nm to 10.7 nm due to the coagulation (Fig. 2j and l). This implies that the photocatalytic activity of i Au/2 ST catalysts is mainly determined by the size of Au NPs. As shown in Table 2, the catalytic activity of ST catalyst used repeatedly decreases significantly compared with fresh ST catalyst [7]. However, Au/2 ST catalysts display much better catalytic stability. This may indicate that the loading of Au NPs could protect the crystal phase structure of ST to some extent, which is the key point to improve the photocatalytic stability of ST catalysts. We also test the stability of 0.5 Au/2 ST in the photocatalytic oxidation reaction of thiophene. Table 3 shows that the photocatalytic activity of 0.5 Au/ST begins to decrease in the fourth cycle, and thiophene conversion in 3 h decreases to 70.0% in the seventh cycle.

We further investigate the photocatalytic behaviors of i Au/2 ST catalysts in the degradation of other pollutants such as RhB, thiol and phenol. Fig. 4a shows the degradation of RhB on fresh i Au/ST catalysts. Among these fresh i Au/ST catalysts, 0.5 Au/2 ST exhibits the highest photocatalytic activity, as it can completely degrade RhB dye within 6 min under visible light irradiation. In contrast, complete degradation of RhB dye on i Au/2 ST (i = 0.1, 1, 2) requires over 9 min. Fig. 4b shows the degradation of RhB on i Au/2 ST catalysts after calcinations at 300 °C in air. The time for complete degradation of RhB dye is obviously much longer compared with fresh i Au/2 ST catalysts. This should be caused by the coagulation of Au NPs during the calcinations process. 0.5 Au/2 ST after calcination still exhibits the highest photocatalytic activity, which can completely degrade RhB dye within 20 min. These results are consistent with those of photocatalytic oxidation of thiophene on i Au/2 ST catalysts.

Additionally, Fig. 5 shows the photocatalytic behaviors of 0.5 Au/2 ST in the degradation of thiol and phenol. The experimental results under the same conditions clearly indicate that thiol and phenol can be completely degraded within 20 min and 1.5 h on 0.5 Au/2 ST, respectively. While on TiO_2 the complete degradation

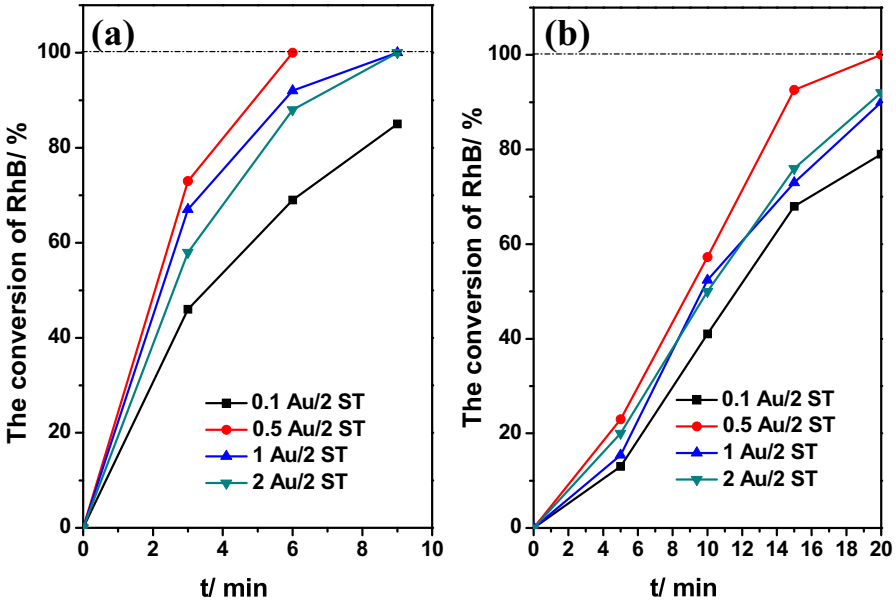

Fig. 4. Photocatalytic degradation of RhB on (a) fresh i Au/2 ST catalysts and (b) i Au/2 ST catalysts after calcinations at 300 °C under visible light irradiation ($\lambda \geq 420$ nm). Reaction conditions: the concentration of photocatalyst: 1 g L^{-1}; C_0 = 5 ppm.

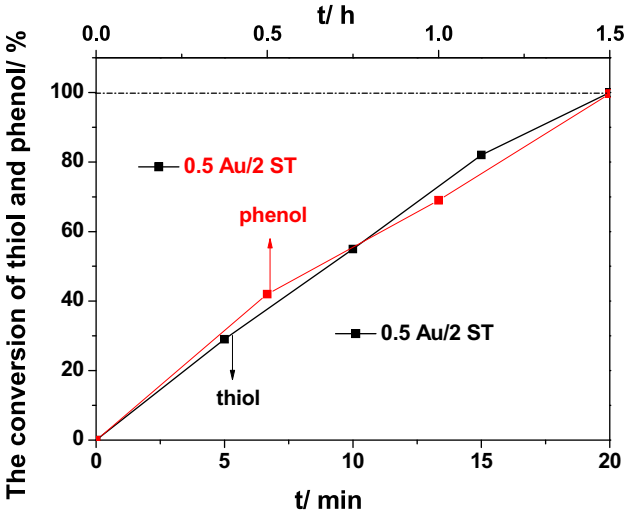

Fig. 5. Photocatalytic degradation of thiol and phenol on 0.5 Au/2 ST catalyst under visible light irradiation ($\lambda \geq 420$ nm). Reaction conditions: the concentration of photocatalyst: 1 g L^{-1}; C_0 = 5 ppm.

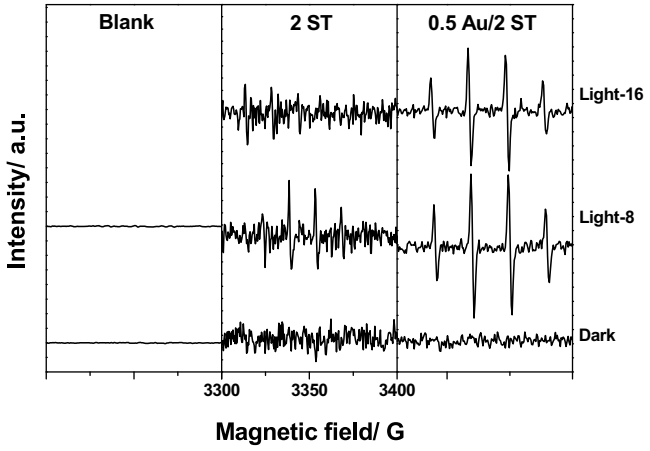

Fig. 6. *In situ* ESR spectra of DMPO-OH generated in the photocatalytic degradation of dye RhB with different photocatalysts. The sample tested without photocatalyst is denoted as "Blank". The signals obtained without light irradiation are denoted as "Dark". The signals obtained after irradiating for 8 min are denoted as "Light-8", similarly, 16 min named as "Light-16".

of RhB, thiol, and phenol need over 2 h, 3 h, and 7 h, respectively. Therefore, these results imply that the photocatalytic activity for degradation of other pollutants such as RhB, thiol, and phenol on TiO_2 can be significantly improved by simultaneous loading Au NPs and sulfation. Both the SPR effect of Au NPs and the surface acidity of ST support play an important role on the enhancement of photocatalytic activity of semiconductors.

3.3. Study on reaction mechanism

To clarify the reaction mechanism of photocatalytic degradation of pollutants on photocatalysts, we employed the *in situ* ESR spin-trap technique (with DMPO) to probe the active oxygen species generated under the illumination. Fig. 6 shows the ESR spectra obtained from the *in situ* photocatalytic degradation reaction of dye RhB. No ESR signals are observed either without photocatalyst or in the dark. After an 8 min illumination in the presence of photocatalysts a signal centered at g = 2.0065 is observed [5,6]. The characteristic quartet peaks in the presence of photocatalysts 2 ST and 0.5 Au/2 ST are assigned to DMPO-OH adduct. The hyperfine splittings are $a_N = a_H = 1.48$ mT, where a_N and a_H denote hyperfine splittings of the nitroxyl nitrogen and a-hydrogen, respectively [42], and the typical 1: 2: 2: 1 lineshape of DMPO-OH adduct is obtained. This provides the evidence of •OH formation in the presence of photocatalysts 2 ST and 0.5 Au/2 ST under the illumination. Besides, the signals of •OH generated after illumination on 0.5 Au/2 ST are much more obvious than those on 2 ST. This implies that much more •OH species are produced in the 0.5 Au/2 ST system. The promoted charge-carrier separation and transport rising from the SPR effect is in favor of the generation of active oxygen species. Additionally, the intensity of the characteristic quartet peaks decrease after a 16 min illumination. This is because of the oxidation of DMPO-OH adduct by h^+ produced during the illumination. Accordingly, we can conclude that •OH which has strong oxidation ability has been involved in the photocatalytic degra-

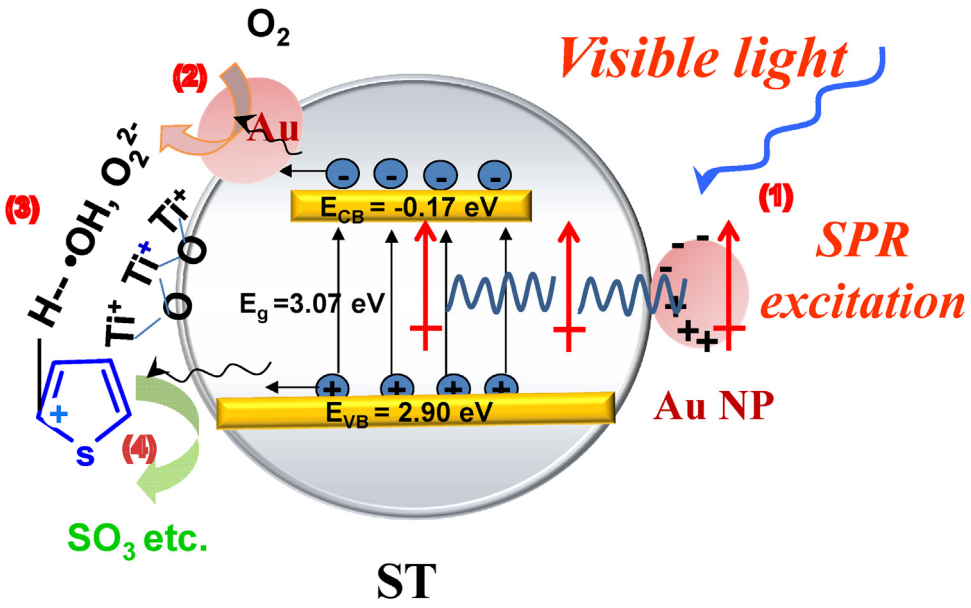

Scheme 1. Schematic description of the mechanism for the photocatalytic oxidation of pollutans (*e.g.* thiophene) on Au/ST photocatalyst.

dation reaction of dye RhB. The aqueous solution is favorable for the transfer and consumption of active oxygen species, which are responsible for the oxidation of pollutants in the system.

A schematic description of the mechanism for the photocatalytic oxidation of pollutants on Au/ST is proposed in Scheme 1. Under the visible light irradiation, ST catalyst can't be self-excited because of the lack of light absorption (Fig. 3). The band edge position (*i.e.* conduction band (CB) and valence band (VB) edges) obtained from Fig. 3b are marked in Scheme 1. However, for Au/ST catalysts, it is proposed that the electromagnetic field mediated plasmonic energy transfer can take the form of a resonant energy transfer (RET) process [30,31,35]. The RET process is proposed to be an alternative, nonradiative mechanism of SPR-induced charge separation in semiconductors. The RET process of Au NPs directly excites electron-hole pairs in the ST semiconductor nonradiatively through the relaxation of the localized surface plasmon dipole. On the other hand, it is known that the Fermi level of Au is 0.5 eV (*versus* NHE) [43], which is lower than the conduction band (CB) edge of ST (−0.17 eV *versus* RHE concluded from Fig. 3b). Then Au NPs on ST surface may act as electron sinks to retard the recombination of the photo generated electrons and holes in ST and thereby increases their lifetime [35,36]. When O_2 is used as the oxidant, photo-generated electron transfer to O_2 on the surface of Au NPs, where superoxide specie •OH is formed when O_2 reacts with the photo-generated electrons. O_2^{2-}, which is the ESR silent species, is also probably formed. In the given mechanism, ST behaves as a typical Lewis acid in the oxidation reaction [7]. It forms an anion radical through an electron acceptor, which can add superoxide species •OH and O_2^{2-} as shown in Scheme 1. It is believed to be the initiation step in the formation of a very reactive unstable oxidized intermediate formed by addition of the anion radical with pollutants molecules [44,45]. Meanwhile, the photo-generated hole transferred to the ST surface could act as an oxidant [45]. •OH is also generated *via* the reaction of OH^- with hole in the reaction. The interaction of the photo-generated hole and •OH with the reactive oxidized intermediate initiate a series of oxidation reactions. The synergistic effect of RET process and Lewis acidic SO_4^{2-}–TiO_2 which capture superoxide species/activate pollutants molecules is beneficial for the efficient transfer of the photo-excited electrons and holes and oxidation of pollutants, being responsible for the highly efficient photocatalytic oxidation of pollutants.

4. Conclusions

The SPR-mediated visible-light-responsive photocatalyst, 0.5 wt.% Au/SO_4^{2-}–TiO_2, can achieve over 99% conversion of pollutants (thiophene, thiol, RhB, and phenol) oxidation under visible light irradiation using molecular oxygen as the oxidant. The light absorption of the photocatalysts can be tuned from the UV-light to near-infrared wavelength range by tailoring the local surface plasmon resonance (LSPR) between Au NPs and ST. The experimental results obtained by XRD, BET and ESR measurements suggest that the crystal phase structure and the ability of electron-hole pairs separation of TiO_2 are greatly improved by Au SPR effect and sulfation process. The synergistic effect of RET process and Lewis acidic SO_4^{2-}–TiO_2 which capture superoxide species/activate pollutants molecules is favorable for the efficient transfer of the photo-excited electrons and holes, and oxidation of pollutants, being responsible for the highly efficient photocatalytic oxidation of pollutants.

Acknowledgments

This work was financially supported by the National Natural Science Foundation of China (Grant No. 21603025, 21506203, 21473186), the Young Thousand Talents Program of China, and the "Strategic Priority Research Program" of the Chinese Academy of Sciences (Grant No. XDA09030103), Chinese Postdoctoral Science Foundation (Grant No. 2016M600218), and Open Project of State Key Laboratory of Catalysis, Dalian Institute of Chemical Physics, Chinese Academy of Sciences (Grant No. N-15-06).

Appendix A. Supplementary data

Supplementary data associated with this article can be found, in the online version, at http://dx.doi.org/10.1016/j.apcatb.2017.06.076.

References

[1] S.J.A. Moniz, S.A. Shevlin, D.J. Martin, Z.X. Guo, J.W. Tang, Energy Environ. Sci. 8 (2015) 731–759.
[2] Z.J. Sun, H.F. Zheng, J.S. Li, P.W. Du, Energy Environ. Sci. 8 (2015) 2668–2676.

[3] B.Y. Zhang, Z.X. Jiang, J. Li, Y.N. Zhang, F. Lin, Y. Liu, C. Li, J. Catal. 287 (2012) 5–12.
[4] A. Samokhvalov, Catal. Rev.-Sci. Eng. 54 (2012) 281–343.
[5] F. Lin, D.E. Wang, Z.X. Jiang, Y. Ma, J. Li, R.G. Li, C. Li, Energy Environ. Sci. 5 (2012) 6400–6406.
[6] F. Lin, Y.N. Zhang, L. Wang, Y.L. Zhang, D.E. Wang, M. Yang, J.H. Yang, B.Y. Zhang, Z.X. Jiang, C. Li, Appl. Catal. B: Environ. 127 (2012) 363–370.
[7] F. Lin, Z.X. Jiang, N.F. Tang, C. Zhang, Z.P. Chen, T.F. Liu, B. Dong, Appl. Catal. B: Environ. 188 (2016) 253–258.
[8] F. Chen, J.C. Zhao, H. Hidaka, Res. Chem. Intermed. 29 (2003) 733–748.
[9] M.Z. Ge, C.Y. Cao, J.Y. Huang, S.H. Li, S.N. Zhang, S. Deng, Q.S. Li, K.Q. Zhang, Y.K. Lai, Nanotechnol. Rev. 5 (2016) 75–112.
[10] M.A. Fox, M.T. Dulay, Chem. Rev. 93 (1993) 341–357.
[11] J. Ryu, W. Choi, Environ. Sci. Technol. 42 (2008) 294–300.
[12] H. Tada, M. Tanaka, Langmuir 13 (1997) 360–364.
[13] Z. Ding, G.Q. Lu, P.F. Greenfield, J. Phys. Chem. B 104 (2000) 4815–4820.
[14] G.H. Li, K.A. Gray, Chem. Phys. 339 (2007) 173–187.
[15] C.M. Ronconi, C. Ribeiro, L.O.S. Bulhoes, E.C. Pereira, J. Alloys Compd. 466 (2008) 435–438.
[16] L.Y. Wang, Y.P. Sun, B.S. Xu, J. Mater. Sci. 43 (2008) 1979–1986.
[17] D.S. Hwang, N.H. Lee, D.Y. Lee, J.S. Song, S.H. Shin, S.J. Kim, Smart Mater. Struct. 15 (2006) 74–80.
[18] A. Testino, I.R. Bellobono, V. Buscaglia, C. Canevali, M. D'Arienzo, S. Polizzi, R. Scotti, F. Morazzoni, J. Am. Chem. Soc. 129 (2007) 3564–3575.
[19] H.P. Xu, Y.P. Sun, J.W. Wang, H.Q. Zhan, X.M. Chen, Rare Metal Mater. Eng. 34 (2005) 1089–1093.
[20] Y. Ma, Q. Xu, X. Zong, D.E. Wang, G.P. Wu, X. Wang, C. Li, Energy Environ. Sci. 5 (2012) 6345–6351.
[21] G. Colon, M.C. Hidalgo, J.A. Navio, Appl. Catal. B 45 (2003) 39–50.
[22] D.S. Muggli, L.F. Ding, Appl. Catal. B: Environ. 32 (2001) 181–194.
[23] H.L. Zhang, H.G. Yu, A.M. Zheng, S.H. Li, W.L. Shen, F. Deng, Environ. Sci. Technol. 42 (2008) 5316–5321.
[24] B. Wang, J.P. Zhu, H.Z. Ma, J. Hazard. Mater. 164 (2009) 256–264.
[25] T. Ishihara, N.S. Baik, N. Ono, J. Photochem. Photobiol. A 167 (2004) 149–157.
[26] J.W. Tang, Z.G. Zou, J.H. Ye, Angew. Chem. Int. Ed. 43 (2004) 4463–4466.
[27] M. Yoshida, A. Yamakata, K. Takanabe, J. Kubota, M. Osawa, K. Domen, J. Am. Chem. Soc. 131 (2009) 13218–13219.
[28] K. Maeda, R. Abe, K. Domen, J. Phys. Chem. C 115 (2011) 3057–3064.
[29] F. Lin, D.E. Wang, Z.X. Jiang, Y. Ma, J. Li, R.G. Li, C. Li, Energy Environ. Sci. 5 (2012) 6400–6406.
[30] F. Lin, Y.N. Zhang, L. Wang, Y.L. Zhang, D.E. Wang, M. Yang, J.H. Yang, B.Y. Zhang, Z.X. Jiang, C. Li, Appl. Catal. B: Environ. 127 (2012) 363–370.
[31] S. Eustis, M.A. El-Sayed, Chem. Soc. Rev. 35 (2006) 209–217.
[32] S.K. Cushing, J.T. Li, F.K. Meng, T.R. Senty, S. Suri, M.J. Zhi, M. Li, A.D. Bristow, N.Q. Wu, J. Am. Chem. Soc. 134 (2012) 15033–15041.
[33] K. Awazu, M. Fujimaki, C. Rockstuhl, J. Tominaga, H. Murakami, Y. Ohki, N. Yoshida, T. Watanable, J. Am. Chem. Soc. 130 (2008) 1676–1680.
[34] C. Hu, T. Peng, X. Hu, Y. Nie, X. Zhou, J. Qu, H. He, J. Am. Chem. Soc. 132 (2010) 857–862.
[35] H. Yuzawa, T. Yoshida, H. Yoshida, Appl. Catal. B: Environ. 115–116 (2012) 294–302.
[36] H. Yuzawa, H. Yoshid, Chem. Commun. 46 (2010) 8854–8856.
[37] Q. Zhang, D.Q. Lima, I. Lee, F. Zaera, M. Chi, Y. Li, Angew. Chem. Int. Ed. 123 (2011) 7226–7230.
[38] S. Naya, A. Inoue, H. Tada, J. Am. Chem. Soc. 132 (2010) 6292–6293.
[39] Z. Liu, W. Hou, P. Pavaskar, M. Aykol, S.B. Cronin, Nano Lett. 11 (2011) 1111–1116.
[40] D.B. Ingram, S. Linic, J. Am. Chem. Soc. 133 (2011) 5202–5205.
[41] I. Thomann, B.A. Pinaud, Z. Chen, B.M. Clemens, T.F. Jaramillo, M.L. Brongersma, Nano Lett. 11 (2011) 3440–3446.
[42] S. Leonard, P.M. Gannett, Y. Rojanasakul, D. Schwegler-Berry, V. Castranova, V. Vallyathan, X.L. Shi, J. Inorg. Biochem. 70 (1998) 239–244.
[43] V. Subramanian, E.E. Wolf, P.V. Kamat, J. Am. Chem. Soc. 126 (2004) 4943–4950.
[44] A. Corma, H. Garcia, Chem. Rev. 102 (2002) 3837–3849.
[45] M.A. Fox, A.A. Abdel-wahab, Tetrahedron Lett. 31 (1990) 4533–4536.